



# Energy distribution during the quasi-static confined comminution of granular materials

Pei Wang<sup>1</sup> · Chloé Arson<sup>1</sup>

Received: 24 July 2017 / Accepted: 18 December 2017 / Published online: 8 January 2018  
© Springer-Verlag GmbH Germany, part of Springer Nature 2018

## Abstract

A method is proposed to calculate the distribution of energy during the quasi-static confined comminution of particulate assemblies. The work input, calculated by integrating the load-displacement curve, is written as the sum of the elastic deformation energy, the breakage energy and the redistribution energy. Experimental results obtained on samples subjected to compression stresses ranging between 0.4 and 92 MPa are used to calibrate the model. The elastic energy stored in the samples is obtained by simulating the compression test on the final particle size distributions (PSDs) with the discrete element method and by extracting the contact forces. A PSD evolution law is proposed to account for particle breakage. The PSD is related to the total particle surface in the sample, which allows calculating the breakage energy. The redistribution energy, which comprises the kinetic energy of particles being rearranged and the friction energy dissipated at contacts, is obtained by subtracting the elastic energy and breakage energy from the work input. Results show that: (1) at least 60% of the work input is dissipated by particle redistribution; (2) the fraction of elastic deformation energy increases, and the fraction of redistribution energy decreases as the compression stress increases; (3) the breakage energy accounts for less than 5% of the total input energy, and this value is independent of the compressive stress; (4) the energy dissipated by redistribution is between 14 and 30 times larger than the breakage energy.

**Keywords** Particulate mechanics · Comminution · Grain breakage · Energy dissipation · Thermodynamics

## 1 Introduction

Particle breakage upon quasi-static comminution is a topic of interest in civil engineering, powder technology and the mineral industry. Many aspects of soil behavior and properties, such as dilation, yielding, shear strength and permeability, are related to particle breakage [16, 22, 40]. Under high compressive stress, particles break and decrease in size. During this process, the total input energy ( $\delta W$ ) is stored in the form of elastic energy in the grains and dissipated by breakage, friction and redistribution, i.e., the production of kinetic energy triggered by crushing [37]. A good understanding of how the energy dissipates during

compression is necessary to formulate sound constitutive models for granular materials. For instance, McDowell and Bolton were able to explain compressibility changes by relating particle crushing to the variations of void ratio and by introducing the breakage energy in the Cam clay model [23]. Based on thermodynamic principles, Collin introduced non-associative flow rules to model friction-induced plasticity in granular materials [8]. Recently, the breakage mechanics theory was formulated to predict the thermodynamic response of crushable granular materials within continuum mechanics [12, 13]. In the theory of breakage mechanics, the evolution of the particle size distribution is used to predict the amount of energy dissipated by breakage, which is fully coupled to the redistribution energy. Within this framework, further developments were proposed to analyze creep, permeability, cementation and the brittle–ductile transition of granular materials [11, 29, 49, 52].

How to calculate the relative fraction of the energy components dissipated during comminution has been

---

✉ Chloé Arson  
chloe.arson@ce.gatech.edu

Pei Wang  
peiwang@gatech.edu

<sup>1</sup> School of Civil and Environmental Engineering, Georgia Institute of Technology, Atlanta, GA, USA

studied for decades both at the grain and at the sample scales, with analytical, numerical and experimental methods. Bolton et al. [5] used a discrete element method (DEM) to analyze the energy distribution during a crushing test performed on a single particle, modeled as an assembly of bonded spheres. The breakage energy was calculated as the total elastic energy stored at the contacts before bonds failed. The energy dissipated by breakage was estimated to be about 10% of the total input energy. The remainder energy was converted into kinetic energy of fragments and then lost by friction and damping. By contrast, in another DEM simulation of particle crushing, the breakage energy was found to be 30% of the total input energy [2]. This difference may come from the properties of the contact bond model, which is difficult to calibrate, and yet largely influences the magnitude of the breakage energy. A variety of contact bond models were proposed to better capture bond breakage [19, 24, 46]. A study combining experiments and numerical simulations showed a strong relationship between bond breakage and strain softening [21]. Some DEM models account for the statistical distributions of bond strengths and particle strengths. However, the distribution of energy at sample scale is still not fully understood [7, 31]. Recently, X-ray micro-tomography was used to measure the area of new material surfaces created during a single particle crushing test [53]. Zhao et al. showed that as breakage proceeds, the extent of material surfaces increases; therefore, the number of potential areas of contact increases, and the proportion of energy dissipated by friction overtakes the energy dissipated by breakage. At the macro-scale, Russell et al. used simplified models to calculate the ratio between the redistribution energy and the breakage energy, which turned out to be stress independent, but dimension dependent: the ratio was 5 to 20 in 1D, 2 in 2D and 1 in 3D [29, 37]. The 3D DEM simulation of a triaxial shear test on crushable soil showed that particle breakage contributed to a small amount to the total energy dissipated, but promoted energy dissipation by inter-particle friction dissipation [47]. Energy distribution was stress dependent, which is in agreement with the results published in [30]. In general, recent results show that energy is mostly dissipated by particle redistribution and inter-granular friction. But there is still no consensus on the relative fraction of the different components of energy dissipated.

In this paper, we present a novel method to calculate the distribution of energy in a granular sample subjected to quasi-static confined comminution. We used results of uniaxial compression tests performed on cylindrical samples of ground shale and sands under both low compressive stress (0.4–2.1 MPa, [30]) and high compressive stress (up to 92 MPa, [27]). The first section explains how we expressed the energy in the form of elastic deformation

energy, breakage energy and redistribution energy. The second section describes the breakage energy model and its calibration. Next, the method to calculate the other energy components is presented. The last section provides a discussion of the results obtained.

## 2 Energy decomposition

Based on the theory of critical state soil mechanics, Roscoe et al. [35] established the following energy balance equation for a soil sample subjected to an increment of mean stress  $\delta p$  and an increment of deviatoric stress  $\delta q$ :

$$q\delta\varepsilon + p\delta v = \frac{\kappa\delta p}{1+e} + Mp\delta\varepsilon, \quad (1)$$

where  $\delta\varepsilon$  and  $\delta v$  are the shear and volumetric strain,  $\kappa$  is the slope of swelling line and  $M = q/p$ . The left-hand side of the equation represents the work done by the mean and deviatoric stresses, while the right-hand side is the sum of the increments of internal energy and dissipated energy. Miura and Yamamoto [26] conducted a series of high-pressure triaxial tests on quartz sand and studied the relationship between the increase in specific surface area  $\Delta S$  and the plastic work  $\delta W_p$ . The ratio  $\Delta S/\delta W_p$  was used as an index of particle crushing and was related to the dilatancy rate. The model was validated later [25] against static triaxial compression tests and repeated triaxial tests on granitic soil. The plastic work included both friction dissipation and breakage energy. McDowell [23] developed further the theory of Roscoe et al. by introducing the breakage energy, expressed as:

$$\Phi_s = \frac{\Gamma \Delta S}{V_s(1+e)} \quad (2)$$

In which  $\Gamma$  is the surface free energy, which remains constant during a confined compression test.

Recently, another form of energy dissipation, called redistribution energy, was introduced in the energy balance equation, in order to account for the rearrangement of grains around crushed particles. The dissipation of redistribution energy is coupled to that of breakage energy, because microstructure rearrangement is triggered by breakage events. The complete energy balance equation was given by [36]:

$$\delta W = \delta\Psi_e + \delta\Phi_p + \delta\Phi_s + \delta\Phi_{\text{redist}} \quad (3)$$

where  $\delta\Psi_e$ ,  $\delta\Phi_p$ ,  $\delta\Phi_s$  and  $\delta\Phi_{\text{redist}}$  represent the elastic energy, plastic dissipation energy, breakage energy and redistribution energy, respectively. Note that plasticity can be due to various processes, such as dislocation creep, dynamic recrystallization, plastic deformation and microfracturing at grain scale [42, 43]. We focus on short-term

isothermal processes and thus ignore thermal softening, volume change and other material property changes induced by temperature variations [39]. We also ignore the transition from brittle to ductile behavior at the grain scale as the coordination number gets higher [48]. Particles are thus considered elastic, i.e., the plastic deformation of the representative elementary volume (REV) is solely due to friction between the grains.

Based on a calibration against two oedometer tests performed on silica sands, it was found that the ratio between the redistribution energy and the breakage energy,  $R = \delta\Phi_{\text{redist}}/\Delta\Phi_S$ , was between 13 and 16. In another study, the breakage energy amounted to 25–30% of the total input energy [2]. A series of uniaxial compression tests conducted on samples of crushable sand of uniform distribution showed that the dissipation of energy by the creation of fracture surfaces depends on the confining stress and that the fracture (or breakage) energy is predominant at low stresses and becomes less predominant at high stresses [30]. The distinction between pure breakage energy, friction energy and redistribution energy is still an open issue to date. Energy is dissipated by redistribution only if breakage events occur in the sample; the dissipation of energy by redistribution is triggered by breakage and increases due to the production of kinetic energy and friction energy. During quasi-static comminution, the production of kinetic energy is negligible in front of the other energy components. That is why in this paper, which focuses on quasi-static comminution, we consider that the redistribution energy includes the friction energy. We use both empirical and numerical methods to calculate the energy dissipated by breakage and the energy dissipated by redistribution. We rewrite Eq. 3 as:

$$\delta W = \delta\Psi_e + \delta\Phi_S + \delta\Phi_{\text{redist}} \quad (4)$$

### 3 Breakage energy

The breakage energy is the energy needed to create new material surfaces when particles break [15]: it is the product of the surface free energy by the grain surface area created by breakage. The surface free energy is a material constant in the order of 0.1–1 Nm/m<sup>2</sup> for rocks and sands [3, 14]. We obtain the grain surface area by calculating the particle size distribution (PSD) and by estimating the surface area of particles within each size range. Note that in the following, we work with PSD expressed in percentage of particle mass. During compression, particles break continuously due to the increasing contact forces. As a result, the number of fines as well as the total surface area of fragments increases with the compressive stress. At

extremely high stress, an ultimate PSD is reached. It was shown empirically that the ultimate PSD can be represented by a fractal distribution [1, 38, 44, 45]:

$$F_u(r) = (r/r_M)^{3-\alpha} \quad (5)$$

where  $\alpha$  is the fractal dimension and  $r_M$  is the maximum particle size. In the following, we use  $\alpha = 0.5$ , which is consistent with experimental results obtained for various materials [44]. In the theory of breakage mechanics, the current PSD  $F_c(r)$  is assumed to be an affine function of the initial PSD  $F_0(r)$  and the ultimate PSD  $F_u(r)$  [11, 13, 29]:

$$F_c(r) = (1 - B_r)F_0(r) + B_rF_u(r) \quad (6)$$

In which  $B_r$  is the breakage variable. A review of recent results obtained during quasi-static comminution indicates that Eq. 6 is not a realistic representation of the PSD evolution, especially for larger particles [10, 20, 27, 30]. To overcome this limitation, we express the current PSD (updated at every step of the crushing process), as follows:

$$F_c(r) = (1 - a)F_b(r) + aF_u(r) \quad (7)$$

where  $F_u(r)$  is the ultimate fractal PSD and  $F_b(r)$  is a uniform distribution, ranging between a size  $r_b$  and the maximum grain size  $r_M$ ;  $a$  and  $r_b$  are fitting parameters. Similar to the breakage parameter  $B_r$  in Eq. 6, the parameter  $a$  represents the evolution of breakage toward the ultimate fractal PSD (from  $a = 0$  to  $a = 1$ ). The model is based on the assumption that the initial PSD is uniform or quasi-uniform, which is a common situation in laboratory experiments [28, 51]. Both parameters  $a$  and  $r_b$  are calibrated against the PSDs obtained at the end of confined comminution tests reported in [30] (tests L1–L4) and in [27] (tests H1–H3). The resulting PSDs of tests L1 and L3,

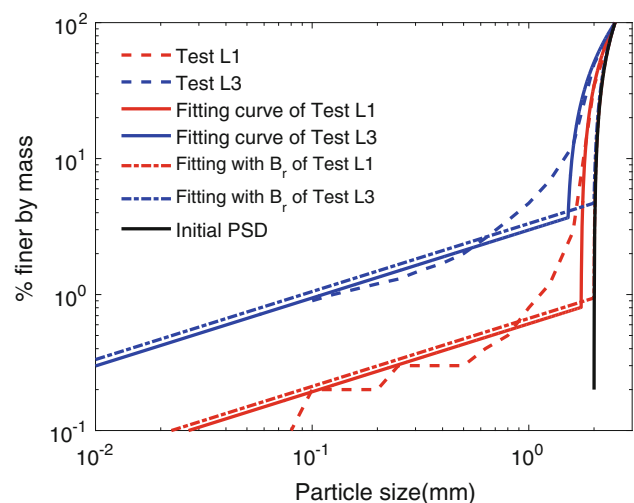


**Fig. 1** Particle size distributions and their best fit according to Eq. 6 ( $B_r$ ) vs. Eq. 7

obtained from Eq. 7, are plotted in Fig. 1. We also show that for larger particles, the final PSD obtained from the breakage mechanics model (Eq. 6) is almost the same as the initial PSD, which results in a 50% error in the calculation of grain surface. The final PSD predicted by Eq. 7 better captures the breakage of large particles. The results of the calibration of parameters  $a$  and  $r_b$  are summarized in Table 1.

Measuring grains’ surface requires characterizing grains’ shapes. The most common method for characterizing the surface area is the Blaine air permeability test, which relates air permeability at given pressure with surface area [4]. Other experimental techniques may lead to different results, in part because surface area depends on surface roughness. For example, gas sorption tests typically give measures that are 2–3 times larger than with Blaine method [41]. Miura found that the grain surface area obtained with Blaine method is close to that that would be obtained by assuming that all grains are spherical: the difference between the two is *at most several tens percent* [25]. That is why, in our model, we consider that particles and fragments are spherical. Let us consider  $N$  size ranges within the interval of sizes  $[r_m, r_M]$  represented in the PSD. At a given load increment, the surface area  $S^*$  of all particles having a radius  $r^*$  comprised between  $r_1^* = r_m + \frac{n-1}{N}(r_M - r_m)$  and  $r_2^* = r_m + \frac{n}{N}(r_M - r_m)$  is calculated as:

$$S^* \approx \sum_{n=1}^N \frac{(F_c(r_2^*) - F_c(r_1^*))M_T S(r^*)}{\rho V(r^*)} \approx \sum_{n=1}^N \frac{(F_c(r_2^*) - F_c(r_1^*))M_T S\left(\frac{r_1^*+r_2^*}{2}\right)}{\rho V\left(\frac{r_1^*+r_2^*}{2}\right)} \tag{8}$$

In which  $S(r^*)$  is the surface of a particle of size  $r^*$ ,  $V(r^*)$  is the volume of a particle of size  $r^*$ ,  $\rho$  is the mass density of the solid grains and  $M_T$  is the total mass of the sample. The current PSD  $F_c(r)$  is obtained from Eq. 7. At each increment, the total number of particles in the sample,  $N_T$ , is calculated by:

$$N_T \approx \sum_{n=1}^N \frac{3M_T(F_c(r_2^*) - F_c(r_1^*))}{4\pi\rho\left(\frac{r_1^*+r_2^*}{2}\right)^3} \tag{9}$$

Equations 7 and 8 allow estimating the energy dissipated by breakage at each loading increment.

### 4 Redistribution energy

Using Eq. 4, the redistribution energy is calculated by subtracting the elastic energy and the breakage energy from the total work input. In this section, we explain how to calculate the total work input and the elastic deformation energy stored in the sample.

#### 4.1 Total input energy

The total input energy is calculated from the force-displacement curve obtained in experiments. For an isothermal uniaxial compression test, the loading platen is the only source of energy input, which has the form:

$$\delta W = F\delta u \tag{10}$$

where  $F$  is the loading force and  $\delta u$  is the increment of displacement. Experimental results of force-displacement relationship for the tests reported in [27, 30] are shown in Fig. 2: the total work input is the area below each curve. Note that in tests L1–L4, samples had different initial void ratios, which explains the different macroscopic stiffnesses observed in Fig. 2.

**Table 1** Parameters  $a$  and  $d_b$  calibrated against uniaxial compression tests

Test	$a$ (-)	$d_b$ (mm)
L1	0.0096	1.744
L2	0.0143	1.707
L3	0.0472	1.518
L4	0.0459	1.495
H1	0.2738	1.106
H2	0.6191	0.878
H3	0.8417	0.998

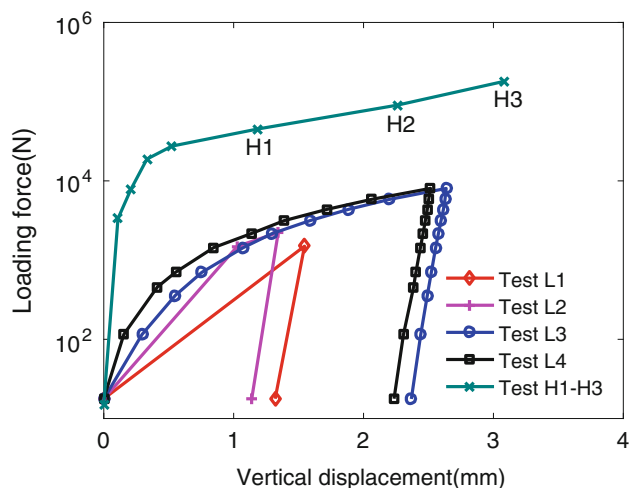


**Fig. 2** Load-displacement curve of uniaxial compression tests performed on crushable sand samples [27, 30]

## 4.2 Elastic energy

We consider that two samples of same PSD subjected to the same external loads have the same statistical distribution of contact forces. This assumption is supported by recent studies that show that the force distribution in a granular assembly follows the same distribution in different samples [6, 34, 50]. The elastic energy was calculated by using the DEM software PFC3D4.0 [17]. First, we generated samples that had the PSD obtained at the end of the confined comminution tests reported in [30] and [27] (Fig. 1). The samples had the same sizes, weight and densities as in the experiments, and the PSDs were modeled with Eq. 7. We subjected these samples to the same boundary conditions as in the experiments. The elastic energy is stored at the contacts between grains. Therefore, with the assumption of constant particle stiffness, the elastic deformation energy of the sample is

$$\Psi_e = 2 \sum_{i=1}^c \frac{F_i^2}{2k_i} \quad (11)$$

where  $c$  is the total number of contacts in the sample,  $F_i$  is the contact force (normal or shear force) and  $k_i$  is the stiffness of the particle (normal or shear stiffness, depending on the orientation of the contact force). In the DEM simulations, we considered a linear relationship between contact force and contact displacement and we used the same value for normal and shear stiffness. Differences in grain packing do not influence the calculation of the elastic deformation energy, as long as the numerical model reproduces the PSD of the samples tested experimentally. We used different stiffness values for L1–L4 tests on the one hand (ground shale) and H1–H3 on the other hand (silica sand). Note that each contact contains two particles, so the elastic energy of the contact is twice that of the particle at that contact.

Another way to obtain the elastic energy of the sample is to find the area below the unloading curve in Fig. 2. However, the value obtained may be 50–60% less than the actual value of the elastic deformation energy, due to the existence of frozen elastic energy [9, 18]. Figure 3 shows

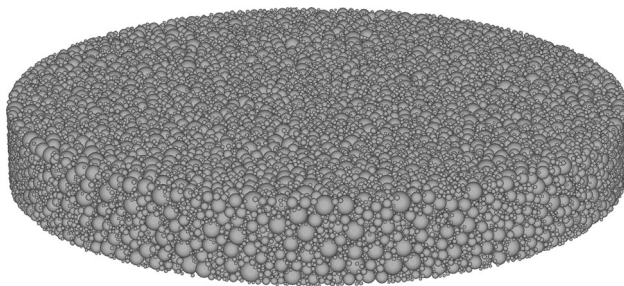


Fig. 3 DEM sample used to simulate the uniaxial compression test H2

the sample used for test H2, after compression. The parameters used in the simulation are reported in Table 2.

After creating the DEM samples, we found that the total number of particles in test L4 was about two million and that there were even more particles in tests H1, H2 and H3. DEM simulations were therefore highly computationally intensive. However, we noted that according to the final PSD obtained in test L4, particles with a diameter less than 0.1 mm accounted for more than 98% of the total number of particles but for less than 1% of the sample weight. Moreover, particles with smaller radius usually have a lower coordination number than larger ones, and force chains usually contain larger particles [33, 34]. The elastic energy of a particle increases with its size: in 2D, the elastic energy stored in a particle increases linearly with its radius [13]; here, in 3D, a quadratic correlation was found between the elastic energy and the particle size (see the example of sample H2 in Fig. 4). As a result, small particles have less elastic energy and in average less contacts than larger ones. Based on these remarks, we performed the DEM simulations with truncated PSDs to increase the computational efficiency: particles with a radius below a radius threshold  $r_t$  were removed from the DEM samples. Details are provided in Table 3. The elastic energy of the removed particles was calculated by using an interpolation relating the elastic energy stored and the particle surface, like in the example of sample H2 in Fig. 4.

After generating the sample, we imposed a controlled velocity on the top platen to apply the uniaxial compression force. The force was continuously monitored during the loading process. When the force reached the value imposed in the experiment, we stopped loading and calculated the total elastic energy stored in the sample from Eq. 11. Note that it was not necessary to consider the crushing of particles here because the goal for this simulation was only to obtain the elastic energy for a specific PSD under a given compressive stress. For each of the 7 tests (L1–L4, H1–H3), three simulations with different random seeds were conducted to guarantee a stable result.

Table 2 Parameters used in the DEM simulations

Variable	Value
Density of sphere ( $\rho$ ): kg/m <sup>3</sup>	2750
Normal and shear stiffness in test L1–L4: N/mm	$4 \times 10^2$
Normal and shear stiffness in test H1–H3: N/mm	$1.5 \times 10^3$
Frictional coefficient of sphere ( $\mu$ )	0.5
Number of particles L1–H3	8000–130,800

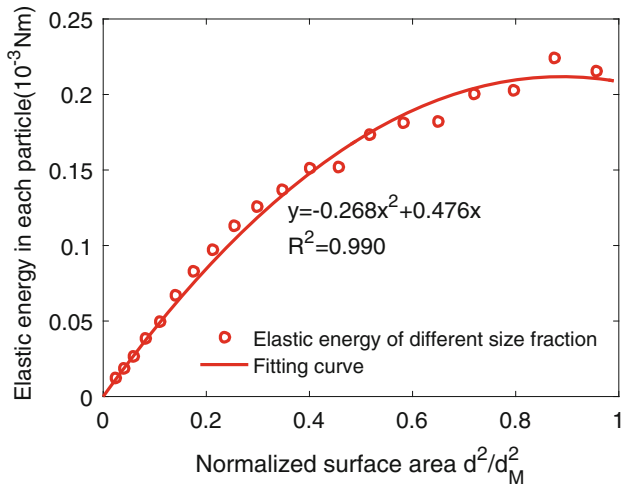


**Fig. 4** Relationship between stored energy in each particle with normalized particle surface area (test H2)

**Table 3** Description of the small particles removed from the DEM samples for the calculation of the elastic energy

Test	Maximum removed size $r_t$ (mm)	% of total mass removed
L1	–	0
L2	–	0
L3	0.11	1
L4	0.11	1
H1	0.14	8
H2	0.17	17
H3	0.20	22

### 5 Results and discussion

DEM simulations allowed calculating the elastic energy stored in each sample under study, at the end of the confined comminution test. Results are shown in Table 4. As

**Table 4** Elastic energy at the end of confined comminution tests

Test	Simulation 1 (N mm/g)	Simulations 2 (N mm/g)	Simulation 3 (N mm/g)	Average (N mm/g)
L1	1.56	1.48	1.58	1.54
L2	2.31	2.28	2.31	2.30
L3	10.38	10.51	10.88	10.60
L4	13.31	13.39	13.35	13.35
H1	249.79	239.23	228.37	238.47
H2	891.40	882.44	881.15	884.99
H3	2352.90	2335.00	2336.55	2341.48

expected, the elastic energy increases with the loading force.

The initial void ratio, compressive stress and increase in specific surface are reported in Table 5 for all tests. As expected, the specific surface increases with the loading force, see Fig. 5. The value of the surface free energy for rocks ranges from 0.3 to 1.0 Nm/m<sup>2</sup> depending on microstructure and environmental conditions [14, 32]. In this research, we use 0.5 Nm/m<sup>2</sup> to calculate the breakage energy. It should be noted that some authors use the fracture surface energy instead of the surface free energy, because measuring surface energy at the scale of the REV is challenged by material heterogeneity, intra-granular micro-cracks and environmental fluctuations. In our simulations, however, we consider that grains are purely brittle and isotropic, under constant environmental condition. The surface free energy introduced in the proposed model is a

**Table 5** Material surface increase during the compression tests

Test	Initial void ratio	Maximum stress (MPa)	Surface increase (mm <sup>2</sup> /g)
L1	1.066	0.39	2224.84
L2	1.015	0.579	2537.18
L3	1.015	2.08	4195.36
L4	0.990	2.09	4280.13
H1	0.6 ± 0.3	23.00	6.23 × 10 <sup>4</sup>
H2	0.6 ± 0.3	46.00	3.10 × 10 <sup>5</sup>
H3	0.6 ± 0.3	92.00	5.60 × 10 <sup>5</sup>

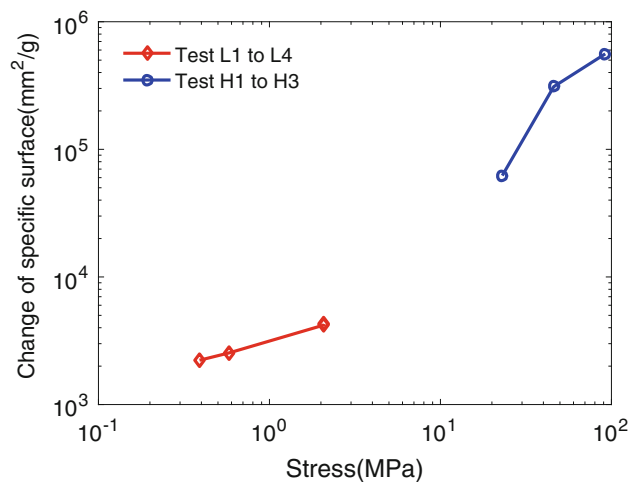


**Fig. 5** Relationship between loading force and surface increase

material constant. A summary of the results on energy distribution is provided in Table 6.

In order to see the role of each energy component during the comminution process, we normalized the data in Table 6 with the corresponding input energy. The results are shown in Fig. 6.

Although the experiments used for model calibration refer to different materials, some interesting conclusions can be drawn from Fig. 6, mainly:

- In all tests, at least 60% of the work input is dissipated by particle redistribution.
- When the compression stress increases from 0.4 MPa (test L1) to 92 MPa (test H3), the redistribution energy decreases from 90 to 60% of the work input, and the elastic deformation energy increases from 10 to 40% of the work input.
- The breakage energy is less than 5% of the work input in all tests, i.e., the energy dissipated by breakage

**Table 6** Energy distribution at the end of the confined comminution tests(unit : N mm/g)

Test	Input energy	Breakage energy	Elastic energy	Redistribution energy
L1	23.82	1.54	1.10	21.18
L2	29.97	2.30	1.25	26.42
L3	74.67	10.60	2.10	61.98
L4	77.37	13.35	2.15	61.87
H1	926.17	31.15	238.47	656.52
H2	3136.33	154.95	884.99	2096.39
H3	6529.99	279.80	2341.48	3908.70

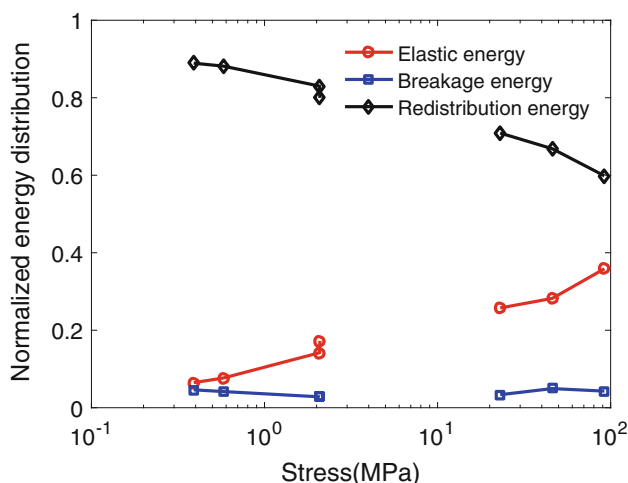


**Fig. 6** Evolution of normalized energy components

seems to represent a constant portion of the work input, regardless of the compression stress.

- The ratio between redistribution dissipation and breakage energy is between 14 and 30 in the tests, which is higher than the ratio of 13–16 found by other authors between friction energy and breakage energy [5, 36, 37]. This result was expected, because in the proposed model, the redistribution energy is the sum of the friction energy and of the kinetic energy of fragments.

## 6 Conclusion

The distribution of energy during confined comminution is calculated for seven particulate assemblies, subjected to compressive stresses ranging from 0.4 to 92 MPa. The work input, calculated by integrating the load-displacement curve, is written as the sum of the elastic deformation energy, the breakage energy and the redistribution energy. The elastic energy stored in the seven samples at the end of the compression tests is obtained by simulating the compression test on the final PSDs with the DEM and by extracting the contact forces. A PSD evolution law is proposed to account for particle breakage, for which parameters are fitted to match the final PSDs obtained experimentally. At each loading step, the current PSD is related to the total particle surface in the sample, which allows calculating the breakage energy. The redistribution energy, which comprises the kinetic energy of particles being rearranged and the friction energy dissipated at contacts, is obtained by subtracting the elastic energy and breakage energy from the work input. Results show that: (1) at least 60% of the work input is dissipated by particle redistribution; (2) the fraction of elastic deformation energy increases, and the fraction of redistribution energy decreases as the compression stress increases; (3) the breakage energy accounts for less than 5% of the total input energy, and this value is independent of the compressive stress; (4) the energy dissipated by redistribution is between 14 and 30 times larger than the breakage energy. This research is expected to increase the fundamental understanding of microstructure changes during confined comminution and to provide a concrete foundation to establish energy based constitutive relationships for granular materials.

## References

1. Abe S, Mair K (2005) Grain fracture in 3D numerical simulations of granular shear. *Geophys Res Lett* 32(5):1–4

2. Afshar T, Disfani MM, Arulrajah A, Narsilio GA, Emam S (2017) Impact of particle shape on breakage of recycled construction and demolition aggregates. *Powder Technol* 308:1–12
3. Arsalan N, Palayangoda SS, Burnett DJ, Buiting JJ, Nguyen QP (2013) Surface energy characterization of sandstone rocks. *J Phys Chem Solids* 74(8):1069–1077
4. ASTM (2016) Standard test methods for fineness of hydraulic cement by air-permeability apparatus. ASTM International, West Conshohocken, PA ASTM C204
5. Bolton M, Nakata Y, Cheng Y (2008) Micro-and macro-mechanical behaviour of dem crushable materials. *Geotechnique* 58(6):471–480
6. Chan S, Ngan A (2005) Statistical distribution of contact forces in packings of deformable spheres. *Mech Mater* 37(4):493–506
7. Ciantia MO, Arroyo M, Calvetti F, Gens A (2016) A numerical investigation of the incremental behavior of crushable granular soils. *Int J Numer Anal Methods Geomech* 40(13):1773–1798
8. Collins I, Houlsby G (1997) Application of thermomechanical principles to the modelling of geotechnical materials. *Proc R Soc Lond A Methods Phys Eng Sci* 453:1975–2001
9. Collins IF (2005) The concept of stored plastic work or frozen elastic energy in soil mechanics. *Geotechnique* 55(5):373–382
10. Coop M, Sorensen K, Freitas TB, Georgoutsos G (2004) Particle breakage during shearing of a carbonate sand. *Géotechnique* 54(3):157–163
11. Das A, Tengattini A, Nguyen G, Einav I (2013) A micromechanics based model for cemented granular materials. In: Yang Q, Zhang J-M, Zheng H, Yao Y (eds) *Constitutive modeling of geomaterials: advances and new applications*. Springer, Berlin, Heidelberg, pp 527–534. [https://doi.org/10.1007/978-3-642-32814-5\\_71](https://doi.org/10.1007/978-3-642-32814-5_71)
12. Einav I (2007a) Breakage mechanics—part II: modelling granular materials. *J Mech Phys Solids* 55(6):1298–1320
13. Einav I (2007b) Breakage mechanics—part I: theory. *J Mech Phys Solids* 55(6):1274–1297
14. Friedman M, Handin J, Alani G (1972) Fracture-surface energy of rocks. *Int J Rock Mech Min Sci Geomech Abstr* 9:757–764
15. Griffith AA (1921) The phenomena of rupture and flow in solids. *Philos Trans R Soc Lond A Contain Pap Math Phys Character* 221:163–198
16. Hardin BO (1985) Crushing of soil particles. *J Geotech Eng* 111(10):1177–1192
17. Itasca (2008) Particle flow code in two dimensions, version 4.0. Itasca Consulting Group, Inc., Minnesota
18. Jefferies M (1997) Plastic work and isotropic softening in unloading. *Géotechnique* 47(5):1037–1042
19. Jiang M, Chen H, Crosta GB (2015) Numerical modeling of rock mechanical behavior and fracture propagation by a new bond contact model. *Int J Rock Mech Min Sci* 78:175–189
20. Lade PV, Yamamoto JA, Bopp PA (1996) Significance of particle crushing in granular materials. *J Geotech Eng* 122(4):309–316
21. Li Z, Wang YH, Ma C, Mok C (2017) Experimental characterization and 3d dem simulation of bond breakages in artificially cemented sands with different bond strengths when subjected to triaxial shearing. *Acta Geotech* 12(5):987–1002
22. McDowell G (2002) On the yielding and plastic compression of sand. *Soils Found* 42(1):139–145
23. McDowell G, Bolton M, Robertson D (1996) The fractal crushing of granular materials. *J Mech Phys Solids* 44(12):2079–2101
24. Meng J, Huang J, Sheng D, Sloan S (2017) Granular contact dynamics with elastic bond model. *Acta Geotech* 12(3):479–493
25. Miura N, O-HARA S (1979) Particle-crushing of a decomposed granite soil under shear stresses. *Soils Found* 19(3):1–14
26. Miura N, Yamamoto T (1976) Particle-crushing properties of sands under high stresses. *Technol Rep Yamaguchi Univ* 1(4):439–447
27. Nakata Y, Hyodo M, Hyde AF, Kato Y, Murata H (2001a) Microscopic particle crushing of sand subjected to high pressure one-dimensional compression. *Soils Found* 41(1):69–82
28. Nakata Y, Kato Y, Hyodo M, HYDE AF, Murata H (2001b) One-dimensional compression behaviour of uniformly graded sand related to single particle crushing strength. *Soils Found* 41(2):39–51
29. Nguyen GD, Einav I (2009) The energetics of cataclasis based on breakage mechanics. *Pure Appl Geophys* 166(10–11):1693–1724. <https://doi.org/10.1007/s00024-009-0518-x>
30. Ovalle C, Dano C, Hicher PY (2013) Experimental data highlighting the role of surface fracture energy in quasi-static confined comminution. *Int J Fract* 182(1):123–130
31. Ovalle C, Voivret C, Dano C, Hicher PY (2016) Population balance in confined comminution using a physically based probabilistic approach for polydisperse granular materials. *Int J Numer Anal Methods Geomech* 40(17):2383–2397
32. Parks GA (1984) Surface and interfacial free energies of quartz. *J Geophys Res Solid Earth* 89(B6):3997–4008
33. Peters J, Muthuswamy M, Wibowo J, Tordesillas A (2005) Characterization of force chains in granular material. *Phys Rev E* 72(4):041,307
34. Radjai F, Jean M, Moreau JJ, Roux S (1996) Force distributions in dense two-dimensional granular systems. *Phys Rev Lett* 77(2):274
35. Roscoe K, Schofield A, Thurairajah A (1963) Yielding of clays in states wetter than critical. *Geotechnique* 13(3):211–240
36. Russell A (2011) A compression line for soils with evolving particle and pore size distributions due to particle crushing. *Géotech Lett* 1(1):5–9
37. Russell AR, Einav I (2013) Energy dissipation from particulate systems undergoing a single particle crushing event. *Granul Matter* 15(3):299–314
38. Sammis C, King G, Biegel R (1987) The kinematics of gouge deformation. *Pure Appl Geophys* 125(5):777–812
39. Semnani SJ, White JA, Borja RI (2016) Thermoplasticity and strain localization in transversely isotropic materials based on anisotropic critical state plasticity. *Int J Numer Anal Methods Geomech* 40(18):2423–2449
40. Tarantino A, Hyde AF (2005) An experimental investigation of work dissipation in crushable materials. *Géotechnique* 55(8):575–584
41. Taylor HF (1997) *Cement chemistry*. Thomas Telford, London
42. Tjioe M, Borja RI (2015) On the pore-scale mechanisms leading to brittle and ductile deformation behavior of crystalline rocks. *Int J Numer Anal Methods Geomech* 39(11):1165–1187
43. Tjioe M, Borja RI (2016) Pore-scale modeling of deformation and shear band bifurcation in porous crystalline rocks. *Int J Numer Methods Eng* 108(3):183–212
44. Turcotte D (1986) Fractals and fragmentation. *J Geophys Res Solid Earth* 91(B2):1921–1926
45. Tyler SW, Wheatcraft SW (1992) Fractal scaling of soil particle-size distributions: analysis and limitations. *Soil Sci Soc Am J* 56(2):362–369
46. Utili S, Nova R (2008) Dem analysis of bonded granular geomaterials. *Int J Numer Anal Methods Geomech* 32(17):1997–2031
47. Wang J, Yan H (2012) Dem analysis of energy dissipation in crushable soils. *Soils Found* 52(4):644–657
48. Wang P, Arson C (2016) Discrete element modeling of shielding and size effects during single particle crushing. *Comput Geotech* 78:227–236



49. Wang P, Arson C et al (2016) Breakage mechanics modeling of the brittle-ductile transition in granular materials. In: 50th US rock mechanics/geomechanics symposium. American Rock Mechanics Association
50. Zhang J, Majmudar T, Tordesillas A, Behringer R (2010) Statistical properties of a 2D granular material subjected to cyclic shear. *Granul Matter* 12(2):159–172
51. Zhang S, Tong C, Li X, Sheng D (2015) A new method for studying the evolution of particle breakage. *Géotechnique* 65(11):911–922
52. Zhang YD, Buscarnera G (2017) A rate-dependent breakage model based on the kinetics of crack growth at the grain scale. *Geotechnique* 67(11):953–967
53. Zhao B, Wang J, Coop M, Viggiani G, Jiang M (2015) An investigation of single sand particle fracture using X-ray microtomography. *Géotechnique* 65(8):625–641